Microfluidics analysis of red blood cell membrane viscoelasticity

Giovanna Tomaiuolo,[ab] Mario Barra,[c] Valentina Preziosi,[a] Antonio Cassinese,[c] Bruno Rotoli[d] and Stefano Guido*[ab]

Received 27th August 2010, Accepted 19th October 2010
DOI: 10.1039/c0lc00348d

In this work, a microfluidic system to investigate the flow behavior of red blood cells in a microcirculation-mimicking network of PDMS microchannels with thickness comparable to cell size is presented. We provide the first quantitative description of cell velocity and shape as a function of the applied pressure drop in such devices. Based on these results, a novel methodology to measure cell membrane viscoelastic properties in converging/diverging flow is developed, and the results are in good agreement with data from the literature. In particular, in the diverging channel the effect of RBC surface viscosity is dominant with respect to shear elasticity. Possible applications include measurements of cell deformability in pathological samples, where reliable methods are still lacking.

Introduction

In microcirculation *in vivo*, red blood cells (RBCs) travel through microvessels with diameter smaller than cell size in order to ensure optimal gas transfer between blood and tissues.[1] In such microconfined flow RBC shape departs from the classical biconcave geometry at rest by taking more fluid dynamic configurations depending on flow rate and microvessel diameter.[2] The high RBC deformability is mainly due to the viscoelastic properties of the cell membrane, especially shear modulus and surface viscosity.[3] Bending resistance is small unless high curvatures are involved,[4] such as in going from biconcave to parachute shapes[5,6] and in slipper-like shapes.[7] An altered RBC deformability is associated with several diseases, such as diabetes, sickle cell anemia and spherocytosis.[1,2] Due to the pathophysiological relevance of RBC deformability, a number of studies on this topic are reported in the literature.[8] The available experimental methods include single cell techniques, such as micropipette aspiration[9–11] and optical tweezers,[12–14] and measurements on whole blood or diluted RBC suspensions, such as blood filtration[15] and ektacytometry.[16] The main drawback of the former techniques is the limited number of cells that can be tested at the same time, thus hindering the acquisition of statistically significant datasets. As far as the whole blood techniques are concerned, the imposed flow geometry is far from the ones actually experienced by RBCs in microcirculation, which makes more difficult to evaluate the clinical relevance of the results.

Recently, microfluidic techniques have been applied to design flow geometries resembling the microvascular network.[17] In principle, microfluidic devices are suitable to testing a large number of cells in a physiologically relevant flow field.[18] By using transparent substrata, such as polydimethylsiloxane (PDMS) and glass, the flow behavior of individual cells has been investigated by video microscopy. Examples from the literature are measurement of cell deformation in healthy donors[19] and diabetes patients,[20] effect of microconfined flow in malaria,[21] flow-induced RBC filtration,[22] determination of pressure drop through a single cell,[23] and measurement of cell size under flow.[24–26] However, to our knowledge microfluidic devices to determine the viscoelastic properties of RBC membrane are still lacking.

In this work, we report on the setup and the quantitative fluid dynamic analysis of a microfluidics device with channel thickness comparable to RBC size. By studying cell deformation in a divergent channel geometry, membrane viscoelastic properties are obtained from the application of the classical Kelvin–Voigt model, which is based on the parallel combination of an elastic spring and a Newtonian damping element.

Methodology

Device fabrication

The microfluidic device is made of PDMS and is fabricated by using soft-lithography techniques with SU-8 as photoresist. The network pattern (Fig. 1) used as a stamp was drawn by a layout program, LASI 7, a commercial software widely used to draw electric microcircuits, and consists of a network of bifurcating

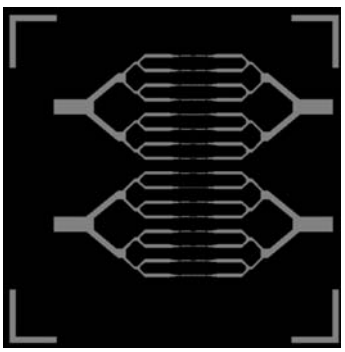

Fig. 1 The geometry used in the microfluidic device.

[a]*Dipartimento di Ingegneria chimica, Università di Napoli Federico II, Napoli, Italy. E-mail: steguido@unina.it; Fax: +39 081-2391800; Tel: +39 081-7682271*
[b]*CEINGE-Advanced Biotechnologies, Napoli, Italy*
[c]*CNR-SPIN and Department of Physics Science, Università di Napoli Federico II, Napoli, Italy. E-mail: antonio.cassinese@unina.it; Fax: +39 081-2391821; Tel: +39 081-7682548*
[d]*Dipartimento di Biochimica e Biotecnologie mediche, Università di Napoli Federico II, Napoli, Italy*

channels of decreasing width (down to 10 micron), including converging–diverging flow sections, to mimic human microcirculation network.

The PDMS microchannels are bond to a glass cover slip by a Corona-treater and the final channel thickness is about 7.5 micron as measured by profilometry.

Experimental setup

Observations are performed through a 100× oil immersion objective by using an optical microscope (Zeiss Axiovert 100) equipped with a motorized translating stage and a focus control (Ludl), and a high speed video camera (Phantom 4.3) operated up to 1000 frames per second (Fig. 2). Venous blood samples are withdrawn from healthy consenting volunteers and used within 4 hours of collection. RBC suspensions used in the experiments are obtained by diluting blood samples 1 : 100 with human albumin supplemented ACD anticoagulant (0.6% citric acid, 1.1% anhydrous dextrose, 2.3% sodium citrate, 96% water). The total pressure drop ΔP_{tot} in the microchannel network is adjusted by changing the distance between a feeding and an exit reservoir connected through plastic tubing to the microfluidics device.

Image acquisition and data analysis

At each pressure drop, a sequence of images (around 10 000) captured by the high speed video camera is recorded on a hard disk. Given the large amount of images to be analyzed, a macro based on the library of a commercial package (Image Pro Plus) has been developed for automated image processing. The output data include RBC center of mass coordinates, velocity and deformation index, DI, defined as the ratio between the sides of a bounding rectangular box enclosing cell contour. Only axisymmetrical RBCs are considered in the following for the sake of comparison with models and experimental data from the literature. The values of pressure drop ΔP_j in each channel of the network are found by calculation since in our experiments only the total pressure drop ΔP_{tot} across the whole microfluidic device is directly known, being imposed as the liquid head between the two reservoirs. In order to calculate ΔP_j, the following Poiseuille-type expression of the flow rate Q_j for a rectangular cross-section channel[27] was used where, once again, the index j refers to a generic channel in the network pattern shown in Fig. 1 and the coordinate system used to describe the flow field and the channel geometry is shown in Fig. 3.

$$Q_j = \frac{W_j H^3}{12\mu}\left(\frac{\Delta P_j}{L_j}\right)\left[1 - \frac{192H}{\pi^5 W_j}\sum_{i=1,3,\ldots}^{\infty}\frac{1}{i^5}\tan h\left(\frac{i\pi W_j}{2H}\right)\right] \quad (1)$$

The term $\frac{W_j H^3}{12\mu}\left(\frac{\Delta P_j}{L_j}\right)$ in eqn (1) is the flow rate in a slit and the term between square brackets is the correction for a finite width channel. The overall flow rate Q is found by imposing that the overall applied pressure drop ΔP_{tot} is equal to the sum of the pressure drops in each channel as calculated from eqn (1). This leads to the following expression for Q according to the splitting geometry shown in Fig. 1:

$$Q = \frac{\Delta P}{\sum_j \frac{12\mu L_j}{W_j H^3}\left[1 - \frac{192H}{\pi^5 W_j}\sum_{i=1,3,\ldots}^{\infty}\frac{1}{i^5}\tan h\left(\frac{i\pi W_j}{2H}\right)\right]^{-1}} \quad (2)$$

This calculation scheme is based on the assumptions that (i) the pressure drops associated with changes in channel direction are negligible with respect to the distributed ones appearing in eqn (1) (this can be confirmed by simple estimates, not shown here for the sake of brevity), and (ii) the contribution of the flowing RBCs to the pressure drop is negligible in the dilute regime investigated in this work (see Secomb *et al.*[4]), (iii) for the same reason, *i.e.*, the high blood dilution, coupled with some bypass around the PDMS chip in the flow cell, the effects of white blood cells, which are 3 orders of magnitude less abundant than RBCs, are negligible as well, and (iv) the dilute blood suspension behaves like a Newtonian liquid. This latter point was confirmed by viscosity measurements performed on glass capillaries, which give a constant value of $\mu = 1.05$ cP independent of wall shear rate.

Results

Constant cross-section channel

We start describing the experimental results from the data obtained in channels having constant cross-section. An example

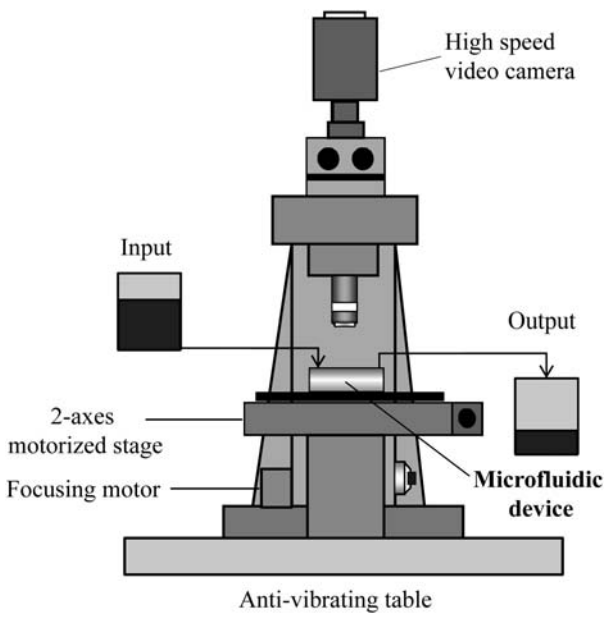

Fig. 2 Schematic of the experimental setup.

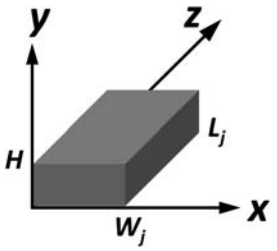

Fig. 3 The coordinate system used to describe the flow field.

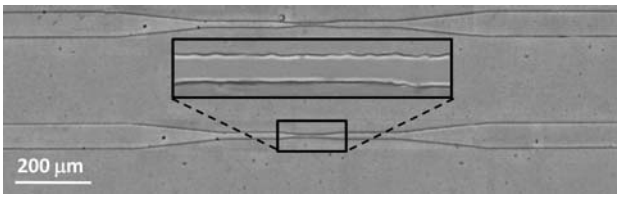

Fig. 4 The straight channel ($W = 10$ micron) selected to analyze RBC motion in a constant cross-section channel.

is presented in Fig. 4, where the enlargement shows the smallest straight channel (width = 10 micron), which has been used to investigate RBC flow behavior.

The data of RBC velocity as a function of the local pressure drop between the ends of the smallest straight channel, $\Delta P/L$, are shown in Fig. 5.

In the same plot data of RBC velocity *vs.* $\Delta P/L$ in circular cross-section microcapillaries of 10 micron inner diameter (which have a cross-section area comparable to that of the rectangular microchannels) are also shown for comparison. It can be noticed that the two sets of data are close to each other, thus showing that the flow behavior of RBCs is similar in the two geometries. This result shows that the effect of the gutters (the regions of the flow field bounded by the curved cell body and the corners of the channel) is not significant for RBCs under confined flow. The effect of the gutters has been found to be important in the case of bubbles flowing in rectangular channels at an intermediate surfactant concentration.[28] A more detailed investigation of this effect in RBCs is outside the scope of this work. Here, it should be noticed that the similarity of RBC flow behavior in rectangular and circular channels provides further support to the use of microfluidics as a relevant experimental model of microcirculation.

Representative images of RBCs flowing in the smallest straight channel are shown in Fig. 6a at two cell velocities. In both cases, cell shapes are deformed with respect to the biconcave rest configuration, being more elongated at increasing cell velocity. As a reference, images of RBCs flowing in circular cross-section

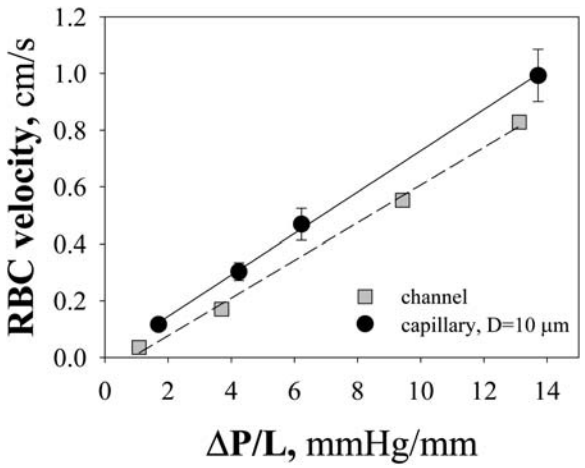

Fig. 5 RBC velocity *vs.* pressure drop per unit length in the straight channel and in a capillary of comparable size ($D = 10$ μm).

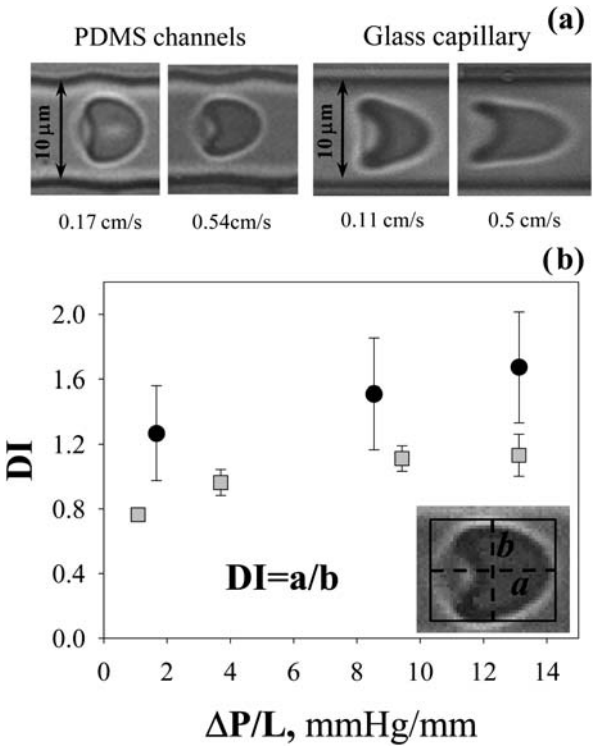

Fig. 6 (a) Representative images of RBCs flowing in rectangular (left) and circular (right) microchannels at a comparable cell velocity. (b) The deformation index, DI, *vs.* $\Delta P/L$ of RBCs flowing in channels (squares) and capillaries (circles) of comparable size.

glass microcapillaries of 10 micron diameter are also shown in the same figure.[29]

In both geometries, RBCs exhibit the typical parachute-like shape found in microcirculation *in vivo*. However, in the PDMS rectangular channels RBCs display a more flattened shape and are more elongated in the *x*-axis due to the channel aspect ratio (=10/7.5). This trend is shown in a quantitative way in Fig. 6b, where the deformation index, DI, defined as the ratio between the sides of a cell rectangular bounding box (see inset), is plotted as a function of $\Delta P/L$. Indeed, at any value of $\Delta P/L$ the deformation index is slightly smaller in the rectangular channels than in the circular cross-section capillaries. In both cases, DI tends to increase with pressure drop and cell velocity. In the rectangular channels the values of DI are smaller than 1 at low $\Delta P/L$, again as expected based on the shapes shown in Fig. 6a.

Divergent channel

In order to measure the viscoelastic properties of the RBC membrane, which are the main factors affecting cell deformability,[30] the flow in the channel region shown in Fig. 7a was investigated. Such region may be divided into three zones: (1) a constant cross-section with $W_I = 10$ μm and $L_I = 25$ μm; (2) a diverging cross-section, with W_{II} ranging from 10 μm to 25 μm and $L_{II} = 100$ μm; (3) a constant cross-section with $W_{III} = 25$ μm and $L_{III} = 65$ μm. The three zones are marked with dashed lines in Fig. 7a. In Fig. 7b RBC velocity is plotted as a function of distance z along the divergent channel centerline at three different pressure drops.

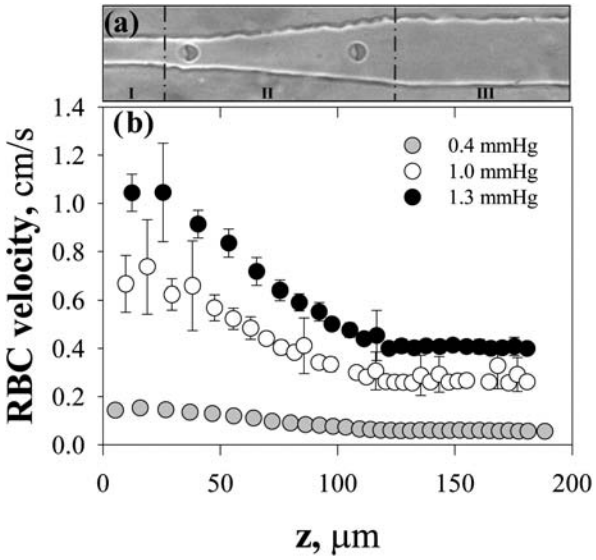

Fig. 7 (a) An image of the channel region used to estimate RBC membrane viscoelastic properties. (b) RBC velocity as a function of z in the same channel region.

The z origin is located halfway in the smallest straight channel. Error bars represent the data standard deviation. Only RBCs with a center of mass moving on the centerline (with a tolerance ±0.3 μm) and thus exhibiting an apparently axisymmetrical shape are considered in this analysis, as shown in the upper image. As expected, RBC velocity decreases with channel width at the same pressure drop and increases with ΔP at any values of z.

For a cell travelling along the centerline, the fluid dynamic action in the divergent channel can be described as a uniaxial compressional stress $\sigma = 3\eta_s\dot{\varepsilon}$, where η_s is the suspending fluid viscosity (1.05 cP) and $\dot{\varepsilon}$ is the strain rate.[31] The latter is equal to the velocity gradient dv/dz at the centerline.[32] In turn, the fluid velocity v at the centerline as a function of z is calculated by dividing eqn (1) by the local cross-section area A in the divergent (which also depends on z as $A = W_{II}H = (W_I + z\tan\alpha)H$, where α is the divergent angle equal to 5°). The calculated velocity gradient as a function of z is shown in Fig. 8 at two extreme values of pressure drop of Fig. 7 (the third one being omitted for the sake of clarity). It can be seen that dv/dz starts from zero in the smaller straight channel, takes a negative minimum and tends to zero again at the larger constant section channel. The extensional stress is then negative in the diverging section, thus corresponding to uniaxial compression, which is the external force acting on the flowing RBCs. Concerning RBC shape, starting from a more elongated configuration in the 10 μm straight channel, a progressive rounding up of the cell body is observed along the divergent length.

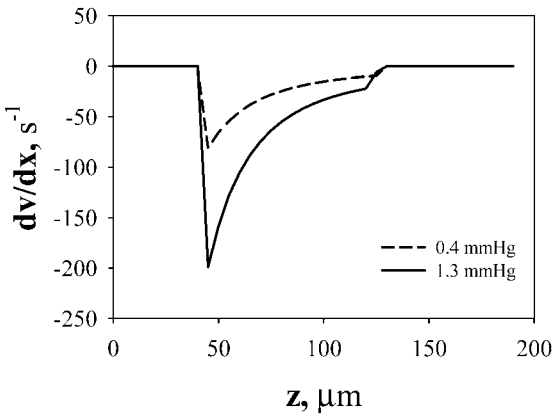

Fig. 8 The calculated velocity gradient as a function of z at two different pressure drops.

A quantitative representation of this behavior can be obtained by plotting the deformation index, DI, as a function of the z coordinate in the divergent channel, as shown in Fig. 9 at the same pressure drops as in Fig. 8.

The deformation index is indeed a decreasing function of z, due to the more rounded shapes as RBCs approach the divergent end. A similar trend is observed in the classical micropipette experiment, where the retraction of a deformed cell *vs.* time is measured after ejection from the capillary.[9,30,33] In our case, the shape change of the RBCs flowing in the divergent channel is elicited by the fluid dynamics of the flow field.

The RBC flow-induced deformation in the divergent channel can be described by using the Kelvin–Voigt model,[30] which is based on the parallel combination of a spring and a dashpot. The two elements are associated with the elastic and viscous response of the cell membrane, respectively. The elastic part is expressed by a shear modulus μ, and the viscous one by a surface viscosity η. We used the following expression of the constitutive equation of the Kelvin–Voigt model:

$$T = \frac{\mu}{2}\left[\left(\frac{\lambda}{\lambda_{fin}}\right)^2 - \left(\frac{\lambda}{\lambda_{fin}}\right)^{-2}\right] + \frac{2\eta}{\lambda}\frac{\partial\lambda}{\partial t} \quad (3)$$

where T is the tension (force/length, see below) acting on the membrane due to the flow field, and λ is the membrane deformation given by the ratio between the initial and the deformed length a of the cell body (see inset of Fig. 6b) in the z direction. λ_{fin} is the value of λ at the end of the divergent channel, and it was found by solving eqn (3) with $\partial\lambda/\partial t = 0$ and $\dot{\varepsilon}$ calculated at the end of the divergent. The membrane tension T is given by

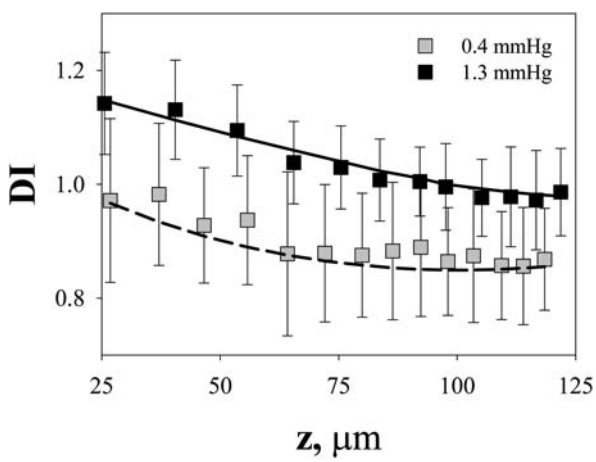

Fig. 9 The deformation index *vs* z in the divergent channel at two pressure drops. Lines are obtained by best-fitting the Kelvin–Voigt model.

$\sigma A_{RBC}/L_{RBC}$, where σ is the flow-generated uniaxial compressional stress acting on RBC membrane, A_{RBC} is the cell area (=135 μm^2) and L_{RBC} is the cell diameter at rest (=8 μm). Eqn (3) was solved by numerical integration for λ and the model parameters μ and η were varied in order to give the best fit of the experimental values of DI in Fig. 9. Indeed, the deformation index is given by the ratio of membrane deformation along the z direction, λ, and membrane deformation along the x direction, which, due to volume conservation, is given by $1/\lambda$. Hence, the deformation index, DI, is equal to λ^2.[30] The best fitting procedure was applied to both datasets of Fig. 9 corresponding to two different values of the pressure drop, and the so obtained values of the model parameters μ and η are 0.006 dyn cm^{-1} and 0.055 cP·cm, respectively. These values are in good agreement with experimental results from the literature (0.006–0.009 for μ, and 0.047–0.1 for η).[2,34–36] The lines in Fig. 9 are the Kelvin–Voigt model predictions based on our fitting parameters, and a good agreement is found.

In order to get more insight into the RBC membrane viscoelastic behavior each term of eqn (3) is plotted *vs.* time in Fig. 10, where T is the membrane tension coming from the external flow field, $T_s^v = \frac{2\eta}{\lambda}\frac{\partial\lambda}{\partial t}$ is the membrane tension associated with the surface viscosity and $T_s^e = \frac{\mu}{2}\left[\left(\frac{\lambda}{\lambda_{fin}}\right)^2 - \left(\frac{\lambda}{\lambda_{fin}}\right)^{-2}\right]$ is the tension due to shear elasticity.

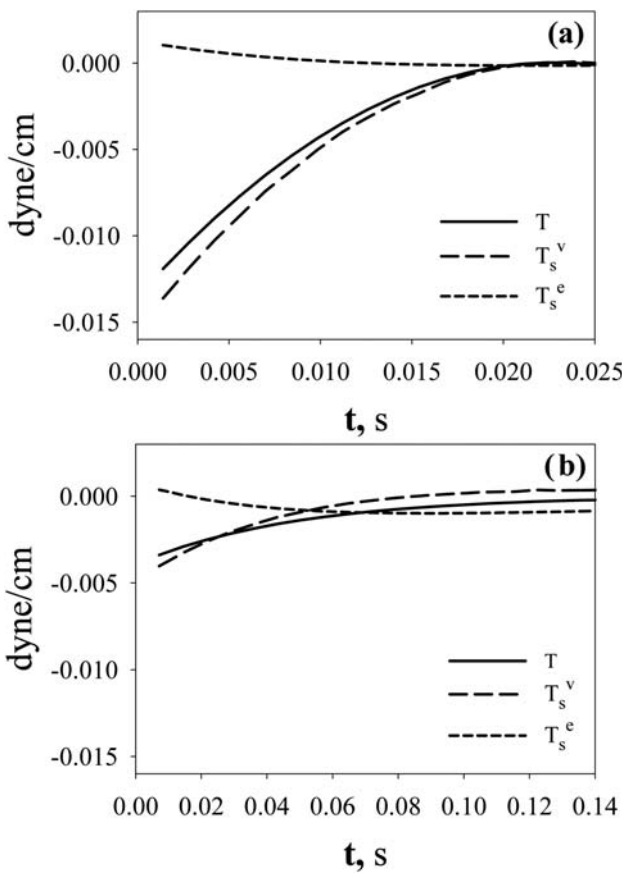

Fig. 10 The three contributes of the tension in the equation of Kelvin–Voigt model at (a) 1.3 mmHg and (b) 0.4 mmHg.

Fig. 10a and b refer to a pressure drop of 1.3 mmHg and 0.4 mmHg, respectively. At both pressure drops the viscous tension is dominant as compared to the elastic one, and this effect increases with pressure drop. In other words, mechanical RBC membrane behavior is mostly governed by the viscous component in the diverging channel. On the contrary, elasticity is dominant in the constant section zones, where viscosity contribution can be considered negligible due to the lack of membrane rotation in axisymmetrical cells.[4] These findings are in line with predictions of Secomb and Hsu[37] for RBC motion through cylindrical micropores based on a time-dependent lubrication equation for the suspending fluid coupled with equations for membrane equilibrium. It can also be noticed that the RBC transit time through the diverging channel at the pressure drop of 0.4 mmHg (~0.15 s) is comparable to RBC characteristic relaxation time, which can be estimated as $\eta/\mu = 0.09$ s. On the other hand, at the higher pressure drop of 1.3 mmHg the RBC transit time is an order of magnitude lower than the relaxation time. Thus, such higher values of pressure drop are best suited to measure RBC surface viscosity.

Conclusions

In conclusion, in this work a microfluidics system to investigate RBC flow in a microcirculation-mimicking network of PDMS microchannels with thickness comparable to cell size has been presented. The observed RBC parachute shapes and velocities are similar to the ones found in glass microcapillaries of similar inner diameter, thus showing that this system is indeed a relevant experimental model to study cell microconfined flow behavior. One of the main results of this work is the development of a novel methodology to estimate cell membrane viscoelastic properties. In particular, in the diverging channel the effect of surface viscosity is dominant with respect to shear elasticity. The main advantages are the small sample volume required, the simultaneous measurement of elastic and viscous parameters, and the continuous flow configuration allowing multiple cells to be examined in the same experiment. Possible applications include the analysis of RBC deformability in pathological situations, for which reliable quantitative methods are still lacking.

Acknowledgements

Financial support from the Italian Ministry of Research under PRIN 2006 program and from the Regione Campania, L.R. 5 2005 is gratefully acknowledged. Support through the BIOMICS—Biomimetic and Cellular Systems ESA topical team was also helpful for stimulating discussions and meeting opportunities. The authors thank Prof. F. Salvatore for supporting this work, Prof. G. Marrucci for useful discussions and M. Cirillo for providing the photomask.

References

1 R. Hoffman and E. J. Benz, *Hematology: Basic Principles and Practice*, Philadelphia, 2000.
2 S. Guido and G. Tomaiuolo, *C. R. Phys.*, 2009, **10**, 751–763.
3 C. Pozrikidis, *Ann. Biomed. Eng.*, 2003, **31**, 1194–1205.
4 T. W. Secomb, R. Skalak, N. Özkaya and J. F. Gross, *J. Fluid Mech.*, 1986, **163**, 405–423.

5 H. Noguchi and G. Gompper, *Proc. Natl. Acad. Sci. U. S. A.*, 2005, **102**, 14159–14164.
6 J. McWhirter, H. Noguchi and G. Gompper, *Proc. Natl. Acad. Sci. U. S. A.*, 2009, **106**, 6039–6043.
7 B. Kaoui, G. Biros and C. Misbah, *Phys. Rev. Lett.*, 2009, **103**, 188101.
8 G. McHedlishvili and N. Maeda, *Jpn. J. Physiol.*, 2001, **51**, 19–30.
9 E. Evans, *Biophys. J.*, 1973, **13**, 941–954.
10 E. Evans and P. La Celle, *Blood*, 1975, **45**, 29–43.
11 K. G. Engstrom and H. J. Meiselman, *Biorheology*, 1995, **32**, 115–116.
12 S. Hénon, G. Lenormand, A. Richert and F. Gallet, *Biophys. J.*, 1999, **76**, 1145–1151.
13 J. Mills, L. Qie, M. Dao, C. Lim and S. Suresh, *Mech. Chem. Biosyst.*, 2004, **1**, 169–180.
14 A. De Luca, G. Rusciano, R. Ciancia, V. Martinelli, G. Pesce, B. Rotoli, L. Selvaggi and A. Sasso, *Opt. Express*, 2008, **16**, 7943–7957.
15 P. Lingard, *Microvasc. Res.*, 1974, **8**, 53–63.
16 M. Bessis, N. Mohandas and C. Feo, *Blood Cells*, 1980, **6**, 315–327.
17 M. Rosenbluth, W. Lam and D. Fletcher, *Lab Chip*, 2008, **8**, 1062–1070.
18 G. Whitesides, *Nature*, 2006, **442**, 368–373.
19 W. Lee, H. Bang, H. Yun, J. Lee, J. Park, J. Kim, S. Chung, K. Cho, C. Chung, D. Han and J. Chang, *Lab Chip*, 2007, **7**, 516–519.
20 K. Tsukada, E. Sekizuka, C. Oshio and H. Minamitani, *Microvasc. Res.*, 2001, **61**, 231–239.
21 J. Shelby, J. White, K. Ganesan, P. Rathod and D. Chiu, *Proc. Natl. Acad. Sci. U. S. A.*, 2003, **100**, 14618–14622.
22 S. Shevkoplyas, T. Yoshida, S. Gifford and M. Bitensky, *Lab Chip*, 2006, **6**, 914–920.
23 M. Abkarian, M. Faivre and H. Stone, *Proc. Natl. Acad. Sci. U. S. A.*, 2006, **103**, 538–542.
24 N. Sutton, M. C. Tracey, I. D. Johnston, R. S. Greenaway and M. W. Rampling, *Microvasc. Res.*, 1997, **53**, 272–281.
25 M. Tracey, R. Greenaway, A. Das, P. Kaye and A. Barnes, *IEEE Trans. Biomed. Eng.*, 1995, **42**, 751–761.
26 S. C. Gifford, M. G. Frank, J. Derganc, C. Gabel, R. H. Austin, T. Yoshida and M. W. Bitensky, *Biophys. J.*, 2003, **84**, 623–633.
27 Z. Tadmor and C. Gogos, *Principles of Polymer Processing*, New York, 1979.
28 M. J. Fuerstman, A. Lai, M. E. Thurlow, S. S. Shevkoplyas, H. A. Stone and G. M. Whitesides, *Lab Chip*, 2007, **7**, 1479–1489.
29 G. Tomaiuolo, M. Simeone, V. Martinelli, B. Rotoli and S. Guido, *Soft Matter*, 2009, **5**, 3736–3740.
30 R. Hochmuth, P. Worthy and E. Evans, *Biophys. J.*, 1979, **26**, 101–114.
31 C. W. Macosko, *Rheology*, New York, 1994.
32 G. Astarita and G. Marrucci, *Principles of Non-Newtonian Fluid Mechanics*, London, 1974.
33 E. Evans, *Biophys. J.*, 1973, **13**, 926–940.
34 R. E. Waugh, PhD thesis, Duke University, 1977.
35 R. E. Waugh and E. A. Evans, *Biophys. J.*, 1979, **26**, 115–131.
36 M. C. Brain, I. Kohn, A. J. McComas, Y. F. Missirlis, M. P. Rathbone and J. Vickers, *N. Engl. J. Med.*, 1978, **298**, 403.
37 T. Secomb and R. Hsu, *Biophys. J.*, 1996, **71**, 1095–1101.